Pacific Northwest
NATIONAL LABORATORY

PNNL-39333

A new capability for investigating the structure and dynamics of liquids at high pressures

May 2026

Greg A Kimmel
Megan K Dunlap
Loni Kringle

U.S. DEPARTMENT of ENERGY

Prepared for the U.S. Department of Energy
under Contract DE-AC05-76RL01830

DISCLAIMER

PACIFIC NORTHWEST NATIONAL LABORATORY
operated by
BATTELLE
for the
UNITED STATES DEPARTMENT OF ENERGY
under Contract DE-AC05-76RL01830

Printed in the United States of America

Available to DOE and DOE contractors from
the Office of Scientific and Technical Information,
P.O. Box 62, Oak Ridge, TN 37831-0062
www.osti.gov
ph: (865) 576-8401
fox: (865) 576-5728
email: reports@osti.gov

Available to the public from the National Technical Information Service
5301 Shawnee Rd., Alexandria, VA 22312
ph: (800) 553-NTIS (6847)
or (703) 605-6000
email: info@ntis.gov
Online ordering: http://www.ntis.gov

PNNL-39333

A new capability for investigating the structure and dynamics of liquids at high pressures

May 2026

Greg A Kimmel
Megan K Dunlap
Loni Kringle

Prepared for
the U.S. Department of Energy
under Contract DE-AC05-76RL01830

Pacific Northwest National Laboratory
Richland, Washington 99354

Summary

Water and aqueous solutions are critical to many areas of science and technology. As a result, tremendous effort has been devoted to understanding them in detail. Despite over a century of research, fundamental questions about water and aqueous solutions remain unanswered. However, an intriguing possibility – that liquid water can exist in two thermodynamically distinct states – has emerged as the most likely explanation. The problem is that experimental confirmation of this hypothesis requires experiments on water at high pressures and low temperatures, conditions in which liquid water only exists briefly before turning into crystalline ice. This project investigated the feasibility of developing a new capability for study water and aqueous solutions under these challenging conditions. The physical constraints, such as the timescales for crystallization and thermal diffusion in supercooled water, were evaluated along with their impact on the design criteria for the instrument. Several basic design options were considered that could meet the technical requirements. The options were also evaluated with respect to their use of commercially available equipment versus the need for custom designs or in-house development. The project identified two viable options to pursue. The first option would use a high-pressure syringe pump in conjunction with fused silica (or sapphire) capillaries. The second option would use a diamond anvil cell. These options can both be used with optical spectroscopies, such as Raman or Infrared.

Acknowledgments

This research was supported by the **PCSD Mission Seed,** under the Laboratory Directed Research and Development (LDRD) Program at Pacific Northwest National Laboratory (PNNL). PNNL is a multi-program national laboratory operated for the U.S. Department of Energy (DOE) by Battelle Memorial Institute under Contract No. DE-AC05-76RL01830.

Acronyms and Abbreviations

DAC	Dimond anvil cell
HDA	High density amorphous (ice)
LLCP	Liquid-liquid critical point
LDA	Low density amorphous (ice)
MD	Molecular dynamics
NML	No Man’s Land

Contents

Figures

1.0 Introduction

It is difficult to overstate the importance of water in many technological and natural processes. While liquid water is ubiquitous, it is also highly unusual.[1] It has been appreciated for decades that the properties of the hydrogen bonding network are at the heart of water's strange behavior,[2] but a detailed understanding has remained elusive and controversial. Two different paradigms for liquid water, which have been in and out of favor several times over the last ~100 years, are that (1) it has a continuous distribution of local structures, or (2) it is a mixture of two distinct local structures. Currently, the leading theories—the liquid–liquid critical point (LLCP) hypothesis and the singularity free scenario—propose that water is a temperature-dependent mixture of high- and low-density structural motifs, placing them in the second paradigm.[1] The high-density (low-density) motif also has a higher (lower) entropy such that is favored at higher (lower) pressures and temperatures.[1, 3] In the LLCP hypothesis, these structural motifs lead to phase separation into high- and low-density liquids, whose coexistence line terminates at a second critical point. However, the critical region, if it exists, is well below the melting point for liquid water. Unfortunately, rapid crystallization has limited the ability to probe the properties of supercooled liquid water below ~230 K (at ambient pressures).

On the other hand, research has shown that water at cryogenic temperatures also has unusual properties.[4-7] For example, two amorphous ices—low-density amorphous (LDA) and high-density amorphous ices —exist and undergo a first-order-like transition.[3, 8] Furthermore, LDA might,[9-12] or might not,[13-15] have a glass transition at ~136 K, above which it transforms into a deeply supercooled liquid. If so, this liquid's possible connection with supercooled water above ~230 K is also controversial.[16-20] Rapid crystallization of the amorphous ices has limited the temperatures for experiments, for example to less than ~160 K for LDA. *The range of temperatures and pressures where rapid crystallization has largely prevented experiments on supercooled water is often called "No man's land" (see Figure 1), and it constitutes a key knowledge gap.*

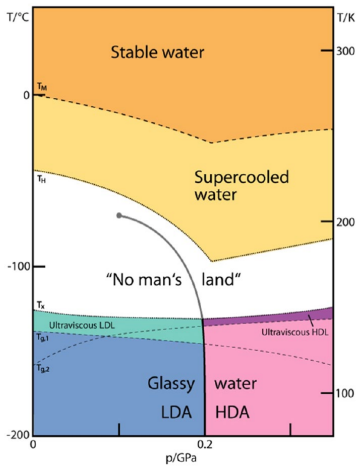

Figure 1. Phase diagram for water, supercooled water, and amorphous ices, which highlights "No man's land."

In addition to the specific questions concerning the physics responsible for pure water's anomalies, it is an essential solvent in countless chemical reactions whose behavior under high-pressure conditions is pivotal for understanding reaction kinetics, and molecular interactions and processes including solvation, dissolution and precipitation. High-pressure environments can alter the hydrogen-bonding network of water, leading to changes in its density, viscosity, and

dielectric properties. Studying aqueous solutions at these conditions enhances our comprehension of phase behavior, critical phenomena, and the thermodynamic properties of water. This knowledge is foundational for theoretical models in physical chemistry and aids in the interpretation of experimental data relevant to numerous applications.

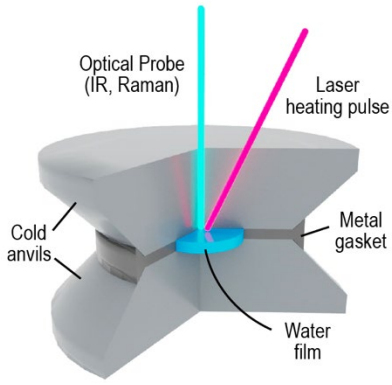

Figure 2. Schematic of how a diamond anvil cell along with pulsed laser heating and optical spectroscopy can be used for experiments on supercooled aqueous solutions at high pressures.

Previously, we developed a novel approach for exploring the properties of supercooled water using nanoscale water films adsorbed on a metal substrate at cryogenic temperatures in ultrahigh vacuum that were transiently-heated into no man's land. That approach used the rapid heating attainable with pulsed lasers in conjunction with the rapid cooling that can be achieved when thin water films are in contact with a macroscopic substrate held at cryogenic temperatures to limit the amount of time a water sample spends in no man's land. However, those experiments are limited to low pressures (~0 MPa!). That basic approach – laser heating and rapid cooling to a cold substrate – guide our concept for experiments at high pressures (see Figure 2). To realize a working version of the concept, there are numerous technical details that need to be addressed. This project investigated the suitability of several possible approaches for conducting experiments on supercooled water at high pressures.

2.0 Apparatus for High Pressure Supercooled Water Experiments

As outlined in the introduction, there is clear need for experiments that explore the properties of water and aqueous solutions in No Man's Land. In the following, we describe the physical constraints that guide the design of the new instrument, and discuss 2 basic design options for conducting the experiments.

2.1 Crystallization time

To prove/disprove the LLT/LLCP hypothesis, ideally one would conduct experiments on bulk samples of water at (metastable) equilibrium that demonstrate one or more of the hallmarks of a first-order phase transition (e.g., density or heat capacity discontinuity, hysteresis) or a critical point (e.g., diverging response function, critical slowing). Those goals place conflicting constraints on the design of the instrument and lead to significant tradeoffs. The first consideration is the desire to achieve metastable equilibrium. The time available is constrained by the nucleation and growth of crystalline ice. The only measurements near the proposed LLCP are experiments on HDA and LDA samples heated to ~100 – 200 MPa were ~50 % crystallized after, τ_{xtal} ~ 10 μs.[21] Other experiments also suggest crystallization occurs on the microsecond timescale. For example, separate experiments on nanoscale droplets with high internal pressures[22] and nanoscale water films at ~ 0 MPa suggest that the maximum ice nucleation rate is J_{max} ~10^{29} #/m^3/s.[23, 24] From classical nucleation theory and Avrami growth kinetics, the characteristic time for crystallization, $\tau_{Av} = (1/JG^3)^{1/4}$ where J is the volume nucleation rate and G is the ice growth rate. For $J = J_{max}$ and G ~ 4 x 10^{-4} m/s at ~215 K,[25] τ_{Av} is ~20 μs, i.e., similar to the other experiment. While this indicates that the timescale needs to be less than ~20 μs for experiments near the proposed LLCP, the available time for experiments as T decreases is expected to get significantly longer due to slower kinetics at lower temperatures.

2.2 Thermal diffusion times in liquid water

Because initially cooling the experimental apparatus will be slow, the sample will start as crystalline ice (either I_h or Ice II, depending on the initial pressure). From that starting point, there are 2 options to produce liquid samples, each of which has its own technical issues to address. In Option 1, the sample can be heated above the melting point and then cooled into the temperature(s) of interest, T_{expt}. In Option 2, the crystalline ice is converted to amorphous ice – either HDA or LDA - through a sequence of (slow) pressure and temperature changes. The amorphous ice can then be heated directly to T_{expt}.

The initial ice samples will be polycrystalline and will also have interfaces with the confining cell. For both option 1 and option 2, sufficient energy for heating the sample can be delivered on the nanosecond timescale with lasers, so heating is not the "rate" limiting step. For option 1, because grain boundaries and interfaces are sites with low or effectively no barriers to melting, melting will be initiated at such sites, and bulk nucleation of the liquid – which has a higher activation barrier – will not be necessary. The time required to melt the ice will be dominated by the melting rate of ice, $G_m(T)$, the time spent above $T_m(P)$, δT_m, and the typical distances between the low barrier sites, x_{defect}. In the Wilson-Frenkel model, $G_m(T) = D(T)F_{therm}(T)/\alpha$, where $F_{therm}(T)$ is the thermodynamic driving force for melting and α is parameter related to the width of ice/water interface. For sufficiently large superheating, $F_{therm}(T)$ ~1 and the melting rate will be proportional to the diffusion rate in water divided by α. Using typical diffusion values for liquid water (~3 × 10^{-9} m^2/s), along with α ~ 0.3 nm (i.e., molecular scale), and x_{defect} ~ 0.1 – 1 μm,

then δT_m ~ 10 – 100 ns. As discussed below, these times are commensurate with the times required to cool the water samples.

For both options, the cooling rate of the water will be largely determined by the rate at which heat diffuses out of the sample. As usual for a diffusion problem, the characteristic time, τ_{diff} , is given by $\tau_{diff} = \frac{x_{diff}^2}{2nD_{th}}$, where n is the dimension for the diffusion, x_{diff}, is the length scale, and D_{th} is thermal conductivity of water. In general, the thermal diffusion coefficient is given by, $D_{th} = \kappa/C_p\rho$, where κ is the thermal conductivity, C_p is the heat capacity, and ρ is the density of the material. The values for these properties are unknown in NML, but we can use known values to get an estimate for D_{th}. Water is largely incompressible, so the densities are all ~ 10^3 kg/m^3 for condensed phases of water. At 0.1 MPa, κ ~ 0.6 and 2.2 J/m/s/K for water and ice, respectively, so ~1 J/m/s/K is appropriate, and for the heat capacity, we can use the value near the melting point C_p ~4200 J/kg/K. With these values, D_{th} ~ 2.4 × 10^{-7} m^2/s, and for target times of 10^{-6}, 10^{-5}, and 10^{-4} s, the corresponding distances are x_{diff} ~0.5, 1.6, and 5 μm, respectively. Because the crystallization times are likely to be approximately 20 μs near the LLCP and longer at lower temperatures, the design should target water samples with thicknesses of a few microns. For example, thick-walled glass capillaries with inner diameters of a few microns are commercially available.

2.3 Laser heating of water

To heat micron scale water samples with a pulsed laser requires matching the laser wavelength to the optical absorbance of water to achieve an acceptable energy absorption profile in the sample – that is one that will lead to an acceptable time- and distance-dependent temperature profile within the sample. The absorption of light in a material is given by $I(z) = I_0 e^{-4\pi\nu k(\nu)z}$, where $k(\nu)$ is the imaginary part of index of refraction and ν is the wavenumber. The energy absorbed from the laser pulse, ΔE, in an increment, dz, in the film is given by $\Delta E = E_{ph} dI = 4\pi E_{ph}\nu k(\nu) I(z) dz$, where E_{ph} is the photon energy. The resulting temperature jump, ΔT, is proportional to the absorbed energy and varies exponentially with distance, $\Delta E = dz\rho C_p \Delta T \propto I(z)$. The choice of laser wavelength requires matching it to the $k(\nu)$ of the material to avoid large gradients in the heating, while also allowing for sufficient absorption to minimize the energy required for the laser pulse to achieve the desired heating. Figure 3 shows the absorption length in water in the wavelength range near the 3-micron band of water along with an estimate of the laser pulse energy needed to raise the water within 100 μm x 100 μm spot by approximately 300 K. The figure also shows the wavelength range for tunable Cr:ZnSe/S lasers pulsed lasers. Lasers of this type with nanosecond pulse durations and output energies of ~ 3 mJ/pulse are commercially available. Note that the parameters chosen for this calculation are conservative. For example, the spot size can probably be smaller and/or smaller temperature jumps employed.

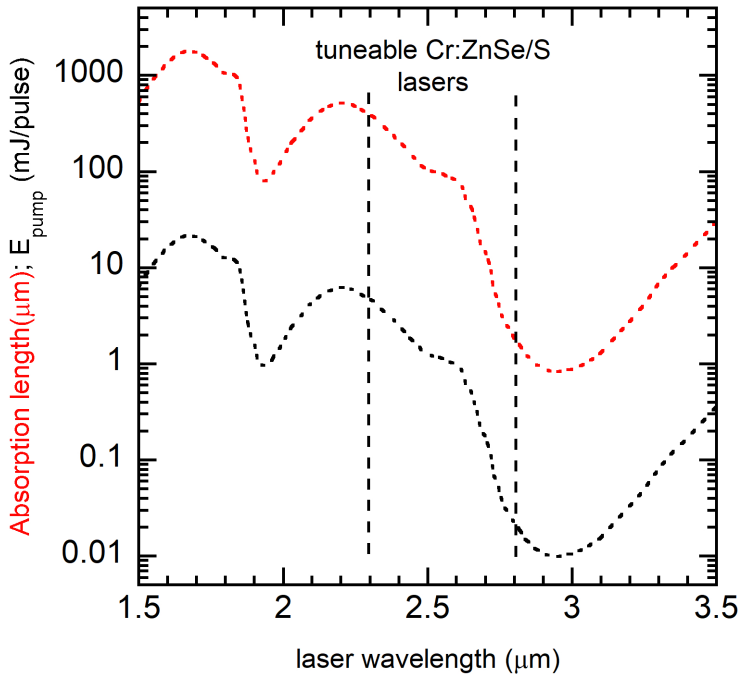

Figure 3. Optical absorption length in water (red line) and the laser pulse energy required to heat a (100 μm)^2 spot by ~300 K (black line). The black dashed lines show the range of wavelengths for a nanosecond, pulse tunable Cr:ZnSe/s laser.

2.4 Syringe Pump + Capillary High-Pressure System

One option for the high-pressure cell is using a syringe pump in conjunction with a “glass” capillary or other cell. Syringe pumps with maximum pressures up to 200 MPa are commercially available (e.g. from Chemyx, HP6 Ultra High-Pressure Syringe Pump). Thick-walled fused quartz or sapphire capillaries with inside diameters of a few microns are available. While connections between the capillaries and the pumps are not trivial, they are available (e.g., VICI Nanovolume Fittings). Advantages of this approach include easier optical access for laser heating and Raman/IR spectroscopy, and easier pressure measurement and regulation. A significant limitation is that maximum pressure for this approach will not permit the formation of HDA directly from crystalline ice. As a result, experiments with this approach will require melting an initially crystalline ice sample with sufficiently rapid cooling to avoid crystallization prior to reaching the desired temperatures in NML.

2.5 Diamond Anvil Cells (DAC)

Diamond anvil cells are another option for the proposed experiments. DACs with optical access for Raman/IR spectroscopies and designed for cryogenic use are commercially available (e.g. Almax-Easylab). The very high pressures attainable with DACs will allow HDA or LDA samples to be produced in situ, by passing the need to first melt crystalline ice, thus allowing experiments where the sample is heated directly to the temperatures of interest. For experiments using that approach, the ability to change the pressure while the system is cold is required. In that case, DACs where the pressure is set with a gas diaphragm are a good option.

One challenge for this approach is that the pressures primarily of interest with respect to the LLCP hypothesis (e.g., ≤ 300 MPa) are on the lower end of the pressures typically used for DACs. At these low pressures, setting and measuring the pressure may be difficult. For example, the shift in wavelength for ruby fluorescence vs pressure is used to measure pressure, but the shift is quite small at pressures The optimal thicknesses for the water samples – a few microns – described above provide a second challenge. Aligning the anvils in a DAC to be that close across the diameter of the anvils would be extremely difficult, and because mistakes, which will fracture the anvils, would be costly. Instead, options that embed water within a suitable pressure medium are needed. For example, mixtures of D_2O and polystyrene beads with the concentration chosen to produce the desired amount of water could be suitable.

3.0 Summary

This report outlines possible experimental strategies for producing and studying liquid water samples under various pressure and temperature conditions necessary for experimental tests fo the Liquid-liquid critical point hypothesis. Two primary methods are discussed: (1) Heating crystalline ice above its melting point and subsequently cooling it, or (2) converting crystalline ice to amorphous ice via controlled pressure and temperature changes, then heating it directly to the desired experimental temperature. The technical details include considerations of polycrystalline ice interfaces, melting kinetics, and the impact of grain boundaries on nucleation and melting rates.

Cooling rates are analyzed through thermal diffusion models, with calculations estimating suitable sample thicknesses for rapid cooling and crystallization avoidance. Laser heating is described in detail, emphasizing the importance of matching laser wavelength to water's optical absorbance for efficient energy transfer. We evaluate high-pressure cell options, such as syringe pumps with glass capillaries and diamond anvil cells (DACs), discussing their advantages, limitations, and suitability for forming high-density amorphous ice. Challenges in sample preparation, pressure regulation, and precise measurement are addressed, along with potential solutions like embedding water in pressure media.

4.0 References

1. P. Gallo, K. Arnann-Winkel, C. A. Angell, M. A. Anisimov, F. Caupin, C. Chakravarty, E. Lascaris, T. Loerting, A. Z. Panagiotopoulos, J. Russo, J. A. Sellberg, H. E. Stanley, H. Tanaka, C. Vega, L. M. Xu and L. G. M. Pettersson, Chemical Reviews **116**, 7463–7500 (2016).
2. F. H. Stillinger, Science **209**, 451–457 (1980).
3. O. Mishima and H. E. Stanley, Nature **396**, 329–335 (1998).
4. K. Amann-Winkel, R. Bohmer, F. Fujara, C. Gainaru, B. Geil and T. Loerting, Reviews of Modern Physics **88** (2016).
5. P. Gallo, T. Loerting and F. Sciortino, Journal of Chemical Physics **151** (2019).
6. T. Loerting and N. Giovambattista, Journal of Physics-Condensed Matter **18**, R919–R977 (2006).
7. N. Giovambattista, K. Amann-Winkel and T. Loerting, in *Liquid Polymorphism*, edited by H. E. Stanley (2013), Vol. 152, pp. 139–173.
8. O. Mishima, L. D. Calvert and E. Whalley, Nature **314**, 76–78 (1985).
9. A. Hallbrucker, E. Mayer and G. P. Johari, Journal of Physical Chemistry **93**, 4986 (1989).
10. G. P. Johari, A. Hallbrucker and E. Mayer, Nature **330**, 552 (1987).
11. G. P. Johari, Journal of Physical Chemistry B **102**, 4711–4714 (1998).
12. C. R. Hill, C. Mitterdorfer, T. G. A. Youngs, D. T. Bowron, H. J. Fraser and T. Loerting, Physical Review Letters **116**, 215501 (2016).
13. C. A. Angell, Science **319**, 582–587 (2008).
14. M. Fisher and J. P. Devlin, J. Phys. Chem. **99**, 11584–11590 (1995).
15. J. J. Shephard and C. G. Salzmann, Journal of Physical Chemistry Letters **7**, 2281–2285 (2016).
16. G. P. Johari, G. Fleissner, A. Hallbrucker and E. Mayer, J. Phys. Chem. **98**, 4719 (1994).
17. R. J. Speedy, J. Phys. Chem. **96**, 2322–2325 (1992).
18. F. W. Starr, C. A. Angell and H. E. Stanley, Physica a-Statistical Mechanics and Its Applications **323**, 51–66 (2003).
19. R. J. Speedy, P. G. Debenedetti, R. S. Smith, C. Huang and B. D. Kay, J. Chem. Phys. **105**, 240–244 (1996).
20. R. S. Smith, J. Matthiesen, J. Knox and B. D. Kay, J. Phys. Chem. A **115**, 5908–5917 (2011).
21. K. H. Kim, K. Amann-Winkel, N. Giovambattista, A. Spah, F. Perakis, H. Pathak, M. L. Parada, C. Yang, D. Mariedahl, T. Eklund, T. J. Lane, S. You, S. Jeong, M. Weston, J. H. Lee, I. Eom, M. Kim, J. Park, S. H. Chun, P. H. Poole and A. Nilsson, Science **370**, 978–982 (2020).
22. A. J. Amaya and B. E. Wyslouzil, Journal of Chemical Physics **148** (2018).
23. Y. T. Xu, N. G. Petrik, R. S. Smith, B. D. Kay and G. A. Kimmel, Journal of Physical Chemistry Letters **8**, 5736–5743 (2017).
24. G. A. Kimmel, Y. T. Xu, A. Brumberg, N. G. Petrik, R. S. Smith and B. D. Kay, Journal of Chemical Physics **150**, 204509 (2019).
25. Y. T. Xu, N. G. Petrik, R. S. Smith, B. D. Kay and G. A. Kimmel, Proceedings of the National Academy of Sciences of the United States of America **113**, 14921–14925 (2016).

Pacific Northwest National Laboratory

902 Battelle Boulevard
P.O. Box 999
Richland, WA 99354

1-888-375-PNNL (7665)

www.pnnl.gov